Astronomy & Astrophysics

The evolution of Lyman α absorbers in the redshift range $0.5 < z < 1.9^\star$

E. Janknecht[1], D. Reimers[1], S. Lopez[2], and D. Tytler[3]

[1] Hamburger Sternwarte, Universität Hamburg, Gojenbergsweg 112, 21029 Hamburg, Germany
    e-mail: [ejanknecht;dreimers]@hs.uni-hamburg.de
[2] Departamento de Astronomia, Universidad de Chile, Casilla 36, Santiago, Chile
    e-mail: slopez@das.uchile.cl
[3] Center for Astrophysics and Space Sciences, University of California, San Diego, MS 0424, La Jolla, CA 92093-0424, USA
    e-mail: tytler@ucsd.edu

ABSTRACT

We investigate the evolution and the statistical properties of the Ly α absorbers of the intergalactic medium (IGM) in the largely unexplored redshift range $z = 0.5$–1.9. We use high-resolution ($R \geq 30\,000$) UV (STIS) and optical (VLT/UVES and Keck/HIRES) spectra of nine bright quasars with $z_{\rm em} < 1.94$. The Ly α lines detected in the lines of sight (LOS) towards these quasars are evaluated with a software package which determines simultaneously the quasar continuum and the line profiles. The main results for the combined Ly α line sample are summarized as follows:

1. The evolution of the number density of the absorbers can be described by the power law $\frac{{\rm d}n}{{\rm d}z} \propto (1 + z)^\gamma$. The number density of the low column density lines ($N_{\rm H\,I} = (10^{12.90}$–$10^{14.00})$ cm^{-2}) decreases with decreasing z with $\gamma = 0.74 \pm 0.31$ in the interval $z = 0.7$–1.9. A comparison with results at higher redshifts shows that it is decelerated in the explored redshift range and turns into a flat evolution for $z \to 0$. The stronger absorbers ($N_{\rm H\,I} > 10^{13.64}$ cm^{-2}) thin out faster ($\gamma = 1.50 \pm 0.45$). The break in their evolution predicted for $z = 1.5$–1.7 cannot be seen down to $z = 0.7$. On the other hand, a comparison with values from the literature for the local number density gives a hint that this break occurs at lower redshift.
2. The distribution of the column densities of the absorbers is complete down to $N_{\rm HI} = 10^{12.90}$ cm^{-2}. It can be approximated by a single power law with the exponent $\beta = 1.60 \pm 0.03$ over almost three orders of magnitude. β is redshift independent.
3. The Ly α lines with lower column densities as well as the higher column density lines show marginal clustering with a 2σ significance over short distances ($\Delta v < 200$ km s^{-1} and $\Delta v < 100$ km s^{-1}, respectively). We do not see any difference in the clustering with either column density or redshift.
4. The distribution of the Doppler parameters has a mean value of $\overline{b} = (34 \pm 22)$ km s^{-1}. This value is typical for the analyzed region. It does not change significantly with z.

Key words. cosmology: observations – intergalactic medium

1. Introduction

It is traditional to decompose spectra of the Ly α forest into individual absorbers that can be fit with Voigt profiles, each with a redshift z, a column density of neutral hydrogen $N_{\rm H\,I}$ and a Doppler parameter b. Examining a sufficiently large number of LOS to background quasi-stellar objects (QSOs), one can derive the distributions of these parameters as well as dependences between them and in this way deduce characteristics of the Ly α forest. Observers have often focused on the evolution of the number density of Ly α lines, usually approximated by the power law

$$\frac{{\rm d}n}{{\rm d}z} = \left(\frac{{\rm d}n}{{\rm d}z}\right)_0 (1 + z)^\gamma \tag{1}$$

(Sargent et al. 1980). At high redshift ($z > 1.5$), the evolution of the strong lines ($\log N_{\rm H\,I} > 14.00$) is steep ($\gamma = 2$–3), transiting

into a flat evolution ($\gamma = 0.1$–0.3) at lower redshift. This abrupt slow-down in the evolution, first detected by observers (Bahcall et al. 1991; Impey et al. 1996; Weymann et al. 1998) and later also seen in simulations (Theuns et al. 1998; Davé et al. 1999), is suspected to happen at $z = 1.5$–1.7.

However, since the apparent break in the evolution rate seems to occur just at the transition from high-resolution optical spectra to low-resolution spectra taken with the HST, the location of this break needs to be confirmed using high-resolution UV spectra. In a previous study, using UV observations of the extremely bright $z_{\rm em} = 1.73$ QSO HE 0515-4414 with a resolution of 30 000, it appeared that the slow-down in the evolution rate did not occur earlier than $z \sim 1$ (Janknecht et al. 2002). However, at low redshift there are few absorbers, and more LOS are necessary.

In this paper we use UV and optical high-resolution data of nine bright quasars to explore the Ly α forest in the redshift range $z = 0.5$–1.9. We believe that this is the first study of the lower column density absorbers in the redshift region $z < 1.5$ using spectra with $R \geq 30\,000$. The paper is organized as follows: in Sect. 2, we explain our selection criteria for the quasars,

Table 1. Parameters of the quasars.

QSO	z_{em}	m_B [mag]
PG 1634+706	1.34	14.9
PKS 0232-04	1.44	16.6
PG 1630+377	1.48	16.5
PG 0117+213	1.50	16.1
HE 0515-4414	1.73	15.0
HE 0141-3932	1.80	16.2
HE 2225-2258	1.89	16.3
HS 0747+4259	1.90	15.8
HE 0429-4901	1.94	16.2

describe the observations and define the redshift ranges that we investigate. Section 3 illustrates how the Ly α lines in the spectra were detected and modelled. After mentioning some interesting individual features in the individual LOS in Sect. 4, we discuss our results in Sect. 5. The main results are summarized in Sect. 6.

2. Observations

2.1. Selection of the quasars

Table 1 gives an overview of the quasars whose spectra we selected to analyze the Ly α forest. We list their emission redshifts z_{em} and their apparent B magnitudes m_B. We selected QSOs with emission redshifts suitable to show the evolution of the Ly α forest at $1 < z < 2$. In Table 2 we give the spectral resolution and the approximate S/N of the spectral regions that we examined. The resolution of the spectra of all nine quasars is high enough to fully resolve all Ly α lines. The S/N varies from one spectrum to the next, and within each spectrum, so the minimum observable column density depends strongly on the spectrum and the wavelength.

2.2. Spectra and data reduction

Because the Ly α line is shifted into the optical for $z \gtrsim 1.5$, a complete analysis of the Ly α forest at median and high redshifts requires both optical and UV spectra. For two of the nine quasars, HE 0515-4414 and HS 0747+4259 (discovery of both objects published in Reimers et al. 1998; for the Ly α forest in the LOS to HE 0515-4414 alone see Janknecht et al. 2002), data in both spectral regions have been obtained: in the UV with HST/STIS with the E230M echelle mode ($R \sim 30\,000$), and in the optical with UVES ($R \sim 50\,000$) for HE 0515-4414 and with Keck/HIRES ($R \sim 38\,000$) for HS 0747+4259.

The sample was extended with the UVES spectra of three bright quasars from the Hamburg ESO Survey taken in the service mode with the VLT. These three were HE 0141-3932, HE 2225-2258 (Wisotzki et al. 2000) and HE 0429-4901 (not yet published). The last was taken with a slit width of $d = 0.8''$, the other two with $d = 1.0''$. The Ly α lines detected in these spectra strengthen the statistics for $1.5 < z < 2.0$.

Finally, the QSO sample was supplemented in the UV ($0.5 < z < 1.5$) with data from the STIS archive. For this purpose the spectra of four quasars – PKS 0232-04 (Shimmins et al. 1966), PG 1630+377 (Noguchi et al. 1980) and PG 0117+213 (Schmidt & Green 1983) from an observing program of B. Jannuzi (HST proposal 8673/cycle 9) and PG 1634+706 (Schmidt & Green 1983) from two programs of S. Burles (7292/7) and B. Jannuzi (8312/8) – were downloaded from the STIS data base. These data were also taken with the

E230M echelle mode resulting in the same resolution applicable to the other STIS spectra.

Table 2 lists the observing dates, exposure times and quality informations for all the QSO spectra.

The data reduction was performed using the pipelines of UVES and STIS on their respective data. The Keck data of HS 0747+4259 was reduced by J. O'Meara using an internal pipeline and the data reduction software package of T. Barlow. For the HE 0515-4414 STIS spectra another rework had to be made: the radiative flux was in places smaller than zero because an inaccurate correction of the noise background of the CCD chips was used in the pipeline. The problem was solved by measuring the signal needed to make the minimum flux in saturated lines zero. A slightly reduced background value (varying from order to order, and extrapolated to orders that lacked saturated lines) was then subtracted from the raw data flux, resulting in positive flux values for the entire spectrum, apart from random photon noise.

The vacuum and the barycentric corrections to the wavelength scales were performed with the data analysis package MIDAS. Multiple exposures of each QSO were added, weighting each flux value $F_{\lambda,i}$ by the inverse variance (noise) σ_i^{-2}.

2.3. Definition of redshift ranges

The sensitivity variations with wavelength of the individual detectors slightly reduce the redshift regions in which the Ly α forest can be examined. For HS 0747+4259, we defined a minimum signal to noise per pixel, averaged over each spectral order, for inclusion in the analysis. This is because the sensitivity of the HIRES chip decreases strongly with decreasing wavelength. Choosing $\langle S/N \rangle > 2$, we ignored the first three orders for HS 0747+4259. Analogously, the first two orders for HE 0429-4901 were left out. The spectrum of PG 1634+706 contains a Lyman limit system, making any detection of Ly α lines below $\lambda < 1865$ Å impossible. We will discuss below how we separate Ly α from other Lyman lines.

We also excluded redshift regions within $\Delta v \sim 2500$–5000 km s^{-1} of the emission redshifts where the ionization of hydrogen is enhanced by the proximity effect. We calculated the maximum redshifts, given in Table 3, from the absolute magnitudes of the QSOs.

For HS 0747+4259, there is a gap of approximately 145 Å between the UV and the optical spectra, while for HE 0515-4414 there is an overlap of roughly 50 Å. In this overlap, we used only lines which can be identified in *both* spectra (nine altogether) and we chose the line parameters from UVES because they are more accurate. Six lines are only found in one spectrum (three in the STIS and three in the UVES spectrum, respectively), all with column densities $\leq 10^{13.20}$ cm^{-2}. We suppose that these are predominantly artefacts.

Absorbers with constant comoving number density and constant proper sizes will have a changing density per unit redshift. We define the absorption distance ΔX so that non-evolving absorbers have a constant density per unit X (Tytler 1982). Assuming the ΛCDM model,

$$\Delta X = \frac{1 + z}{\sqrt{\Omega_M(1 + z) + \frac{\Omega_\Lambda}{(1+z)^2}}} \, \Delta z \qquad (2)$$

(Misawa et al. 2002), where Ω_M and Ω_Λ are the density parameters for matter and for dark energy, respectively.
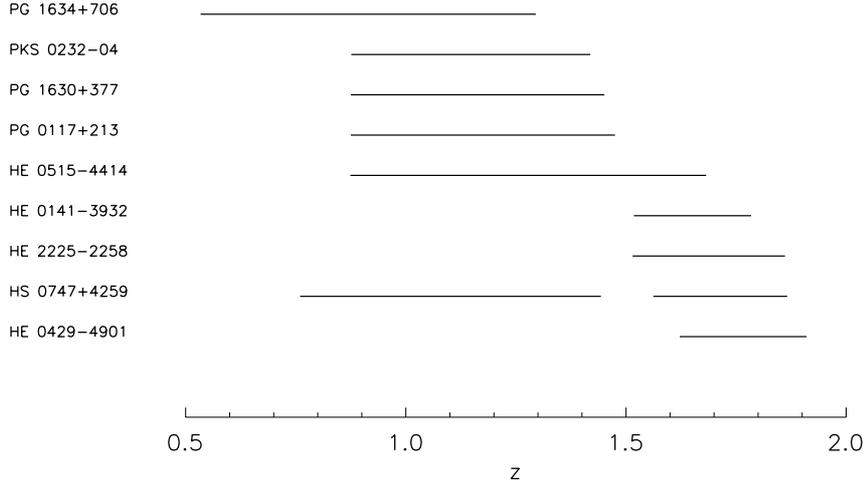
Fig. 1. Visualization of the analyzed redshift ranges of our quasars.

Table 2. Log of the observations used in this study.

QSO	Telescope/spectrograph	Observing date	Exposure time [s]	R	S/N per pixel
PG 1634+706	HST/STIS	May 5, June 26, 1999	26 400–29 000	30 000	5–50
PKS 0232-04	HST/STIS	Feb. 6, 8, 2001, Jan. 19, 2002	41 900	30 000	4–15
PG 1630+377	HST/STIS	Feb. 27, Oct. 8, 12, 2001	34 100	30 000	5–11
PG 0117+213	HST/STIS	Dec. 31, 2000–Jan. 12, 2001	42 000	30 000	4–12
HE 0515-4414	HST/STIS	Jan. 31–Feb. 2, 2000	31 500	30 000	~10
	VLT/UVES	Oct. 7, 2000–Jan. 3, 2001	31 500	50 000	10–50
HE 0141-3932	VLT/UVES	July 19, Aug. 14–24, 2001	39 600	40 000	~25
HE 2225-2258	VLT/UVES	June 17–28, July 14, 15, 2001	41 800	40 000	~25
HS 0747+4259	HST/STIS	Sep. 6, 12–16, 2001	54 200	30 000	3–10
	Keck I/HIRES	Feb. 28, Mar 1, 2001	5 400	38 000	3–12
HE 0429-4901	VLT/UVES	Feb. 1, Mar 18, 19, 2001	10 800	50 000	~8

Table 3. Evaluated redshift ranges and absorption distances of the quasar LOS and numbers of Ly α lines n detected in the indicated spectral regions.

QSO	$\lambda\lambda$ [Å]	z range	Δz	ΔX	n
PG 1634+706	1865–2790	0.534–1.295	0.761	1.665	195
PKS 0232-04	2280–2941	0.876–1.419	0.544	1.309	128
PG 1630+377	2279–2980	0.875–1.451	0.577	1.396	118
PG 0117+213	2279–3009	0.875–1.475	0.600	1.460	160
HE 0515-4414	2278–3260	0.874–1.682	0.808	2.034	220
HE 0141-3932	3061–3384	1.518–1.784	0.266	0.745	97
HE 2225-2258	3057–3478	1.515–1.861	0.346	0.979	130
HS 0747+4259	2140–2970	0.760–1.443	0.683	1.615	110
	3115–3484	1.562–1.866	0.304	0.864	79
HE 0429-4901	3188–3538	1.622–1.910	0.288	0.830	88
Σ			5.176	12.897	1325

Given a set of QSO spectra, in general there are multiple LOS which sample a specific redshift range. We take this into account by converting the z into X values and summing the ΔX values to obtain the total absorption distance.

Table 3 shows the wavelength and redshift regions (columns two and three) that we investigated for all quasars after removal of the proximity zones and low S/N orders. The fourth and fifth columns give the computed redshift path Δz and the absorption distance ΔX. The total absorption distance for all nine examined quasar LOS is $\Delta X = 12.897$. In the sixth column we give the number of detected Ly α absorption lines, 1325 altogether.

In Fig. 1 we show the redshift intervals of the LOS, while in Fig. 2 we show the distribution of all 1325 Ly α lines as a function of redshift and column density, giving qualitative

information on the contents of the sample. It can be clearly seen that the redshift interval analysed in this paper is well sampled.

3. Voigt profile fits

The analysis of absorption lines detected in quasar spectra is usually performed in three steps. First the lines have to be identified as certain atomic transitions that have been redshifted to the observed wavelengths. Then they are modelled. Finally they are accepted or rejected for the line sample.

For the line identification we used the empirical fact that the H I Doppler parameter b is rarely smaller than 15 km s^{-1} and never ≤ 10 km s^{-1}, while for metal lines almost always $b \leq 10$ km s^{-1}. In most cases, it can a priori be discriminated between H I and metal lines by inspecting the line width.
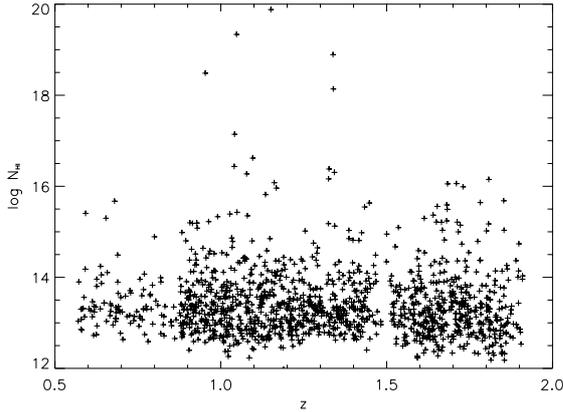
Fig. 2. Distribution of all 1325 Ly α lines as a function of redshift and column density.

The identification strategy was as follows. After rejecting the interstellar lines, the strongest Ly α absorbers (i.e., the lines with the highest column densities) were picked out. Having identified a Ly α line at the wavelength $\lambda_{\mathrm{Ly}\alpha}$ with a H I column density $\log N_{\mathrm{H\,I}} \gtrsim 14.00$ (the exact lower bound depending on the S/N), the associated Ly β can in principle be found at the same redshift. For higher column density systems, further transitions of the Lyman series (with monotonically decreasing line strength) can be detected.

Using the redshifts of the strongest H I systems, we could search for metal lines. We found many additional metal lines at the redshifts of the common C IV 1548/1550 doublets.

The absorption line list derived in this way still contains a few unidentified lines, noise dips interpreted as absorption lines by mistake, unidentified blends, and wrong identifications. However, at these low redshifts, and especially in the high-resolution UVES spectra with their high S/N we guess that such errors are less than 5% of the total list. Besides, the unidentified or wrongly identified lines are typically those with very low column densities and/or low Doppler parameters, which are either rejected by applying the significance level (see below) or do not belong in our Ly α line sample. On the other hand, the blends are a problem that is easily underestimated.

We fit the Ly α lines with two different programs: the lines found in the HST/STIS and VLT/UVES spectra of HE 0515-4414 were fit with the MIDAS software package FITLYMAN (Fontana & Ballester 1995), which needs a normalized spectrum as input. In order to obtain this, the effective background continuum of the quasar was defined with MIDAS by specifying points in line-free regions and fitting these by a polynomial. An improvement to FITLYMAN is the program CANDALF developed by R. Baade. In CANDALF, the continuum is determined *simultaneously* with the line fitting procedure. With this parallel approach, the continuum can also be defined reliably in spectral regions where it is hidden by a high line density. CANDALF was used for the analysis of all quasar spectra except for HE 0515-4414 whose spectra were already fit before the development of CANDALF.

Extensive investigations of complex absorption line ensembles, several with partly blended atomic transitions and lines of multiplets fit simultaneously, were carried out with both programs to check their consistency. The comparison of the ionic parameters determined with FITLYMAN and with CANDALF showed that they were consistent within 1σ in almost all cases. CANDALF converges more easily compared with FITLYMAN in regions with high line densities, finds the global fit minimum

with larger probability, and its fit errors are a little bit smaller; however the choice of the fitting program does not have any significant influence on the results of the analysis of the whole Ly α sample (Sect. 5).

FITLYMAN and CANDALF both assume Voigt profiles convolved with the instrumental profile. The programs adjust three independent parameters per line to minimize the χ^2: z, $N_{\mathrm{H\,I}}$ and b which comprises the thermal and the turbulent broadening of the lines. The general fit strategy, especially for blends, was to start with a single line and to add further components as long as the χ^2 decreased significantly. Different atomic transitions of the same ion were fit with identical values for $N_{\mathrm{H\,I}}$, b and z. This is particularly important for the saturated Ly α lines ($\log N_{\mathrm{H\,I}} \gtrsim 13.50-14.00$) lying in the flat part of the curve of growth where $\log N_{\mathrm{H\,I}}$ is very inaccurate. In addition the number of subcomponents of an absorber is harder to determine at higher column densities. However, the fragmentation of an absorber into several weak absorbers can be seen in Ly β and other Lyman series lines because these lines are usually not saturated and give more accurate parameters.

Since the lower column density lines can hardly be distinguished from the photon noise, it is usual practice to define the significance level

$$SL = \frac{W}{\sigma_W} \qquad (3)$$

where W is the observed equivalent width of the line and σ_W is the 1σ error of W (Young et al. 1979). Usually the approximation $\sigma_W \sim \frac{FWHM}{\langle S/N \rangle}$ with $\langle S/N \rangle$ being the average signal to noise in the region of the considered absorption line is used (Tytler et al. 1987; Caulet 1989). This describes the error caused by the determination of the continuum. However it neglects the fit error (Sembach & Savage 1992). Here we performed an extended estimation of SL that includes the fit error:

$$\sigma_W \sim \sqrt{\left(\frac{\lambda}{R\langle S/N \rangle}\right)^2 + \sigma_{\mathrm{Fit}}^2}. \qquad (4)$$

Because of this extended error estimation, we chose a comparatively low selection threshold $SL > 1$. With this selection criterium about 5% of all presumed Ly α lines were rejected from the sample. However, we did not reject Ly α lines that are at redshifts where metal lines can be seen.

The full list of all 1325 detected and modelled Ly α lines with their fit parameters and errors are available in electronic form at the CDS.

4. Individual LOS

Before we analyze the Ly α line sample from all nine quasar LOS in Sect. 5, we briefly mention some interesting characteristics in the individual LOS.

4.1. HE 0515-4414

In the LOS to the quasar HE 0515-4414 a damped Ly α (DLA) system can be seen at $z \sim 1.15$. Because of this absorber and the brightness of the quasar ($m_B = 15.0$ mag), it was already a topic of several studies with different goals by the Hamburg group (de la Varga et al. 2000; Reimers et al. 2001, 2003; Janknecht et al. 2002; Quast et al. 2002, 2004, 2006; Levshakov et al. 2003).
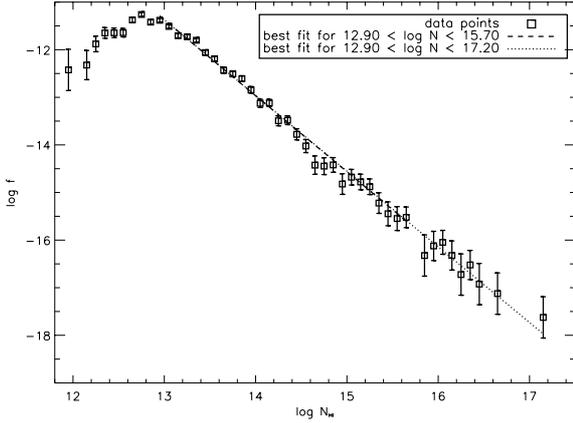
Fig. 3. Distribution of the Ly α column densities in intervals $\Delta \log N_{\mathrm{H\,I}} = 0.1$, statistical error of $\log f$ and fits to the distribution for different fit regions. For the calculation of the fit parameters, the data points were weighted with their error.

4.2. HS 0747+4259

The metal line spectrum of HS 0747+4259 has been studied in a separate paper (Reimers et al. 2006) which concentrated on the O VI absorbing systems in this LOS.

4.3. HE 0141-3932

HE 0141-3932 is an unusual quasar in several respects: its spectrum contains – atypical for quasars – an extremely weak Ly α emission line. In addition the emission lines of different ions give rather different redshifts, depending on the degree of ionization (e.g., Tytler & Fan 1992). Furthermore, the quasar has several associated absorption systems presumably built by gas ejected from the QSO. The chemical composition of this gas is rather atypical. These special characteristics of HE 0141-3932 are discussed in detail in Reimers et al. (2005) and in Levshakov et al. (2005).

5. Analysis and discussion

5.1. Column density distribution

The differential distribution function of the hydrogen column densities $f(N_{\mathrm{H\,I}})$ is usually defined as the number n of Ly α absorption lines per column density interval $\Delta N_{\mathrm{H\,I}}$ and per absorption distance ΔX (ΔX from (2); Tytler, 1987). Since our data contains more than one LOS, we need the sum of the individual ΔX_i over all LOS:

$$f(N_{\mathrm{H\,I}}) = \frac{n}{\Delta N_{\mathrm{H\,I}} \, \Sigma_{i=1}^{j} \Delta X_i}. \tag{5}$$

In Fig. 3 the distribution function for the lines of all nine LOS is plotted against the column density. Note that the error bars on $\log f$ increase with increasing column density because of the decreasing number of lines. Figure 3 shows that the data points at the highest column densities have a low statistical significance. The fits plotted in this diagram were derived by weighting the data points with $1/\sigma_{\log f}^2$. The absorption lines were binned in intervals $\Delta \log N_{\mathrm{H\,I}} = 0.1$. As expected, the linearity of $\log f$ breaks off at low column densities. This presumably reflects a selection effect: the weak lines are hidden by the the noise of the spectra.
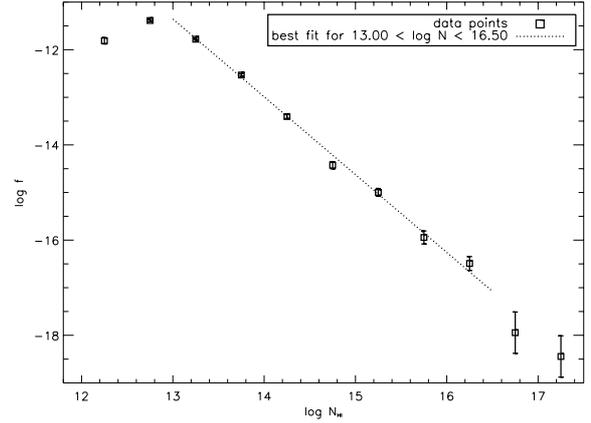

Fig. 4. Distribution of the Ly α column densities in intervals $\Delta \log N_{\mathrm{H\,I}} = 0.5$, statistical error of $\log f$ and fit to the distribution. The data points were weighted with the error for the fit.

Table 4. Fit parameters of the column density distribution for different boundary conditions. Given are (*from left to right*): the $\log N_{\mathrm{H\,I}}$ range of the data points considered in the fit; the interval width; the fit parameters $\log A$ and β with their 1σ errors.

$\log N_{\mathrm{H\,I}}$	$\Delta \log N_{\mathrm{H\,I}}$	$\log A$	β
12.90–15.70	0.1	9.4 ± 0.3	1.60 ± 0.03
12.90–17.20	0.1	9.3 ± 0.3	1.59 ± 0.02
13.00–15.50	0.5	10.0 ± 0.4	1.64 ± 0.03
13.00–16.50	0.5	9.9 ± 0.3	1.63 ± 0.02

In general, the column density distribution function can be well approximated by the power law

$$f(N_{\mathrm{H\,I}}) = A \cdot N_{\mathrm{H\,I}}^{-\beta}, \tag{6}$$

where β is the (negative) slope and $\log A$ is the intercept of the logarithmic representation of $f(N_{\mathrm{H\,I}})$.

We set a completeness limit $\log N_{\mathrm{H\,I}} = 12.90$ for the analyzed line ensemble, while we chose $\log N_{\mathrm{H\,I}} = 15.70$ for the upper limit (see Fig. 3). Using these boundaries and fitting the model (6) to the column density distribution, we derived $\log A = 9.4 \pm 0.3$ and $\beta = 1.60 \pm 0.03$. This result is consistent with other studies of the column density distribution at lower $\log N_{\mathrm{H\,I}}$ at comparable z: Dobrzycki et al. (2002) found $\beta \leq 1.6-1.7$ performing a curve of growth analysis. Hu et al. (1995) determined $\beta = 1.46$ for $\log N_{\mathrm{H\,I}} = 12.30-14.50$, and Kim et al. (2001) derived an exponent $\beta = 1.70-1.74$ with varying column density regions.

Occasionally it has been claimed that at least two power laws are necessary to accurately describe the column density distribution over the observed range of column density (Carswell et al. 1987; Giallongo et al. 1993; Meiksin & Madau 1993; Petitjean et al. 1993; Penton et al. 2004). If we extend our fit region to higher column densities ($\log N_{\mathrm{H\,I}} = 12.90-17.20$), the distribution does not flatten ($\beta = 1.59 \pm 0.02$). However, our sample is too small at large column densities to see minor changes in this $N_{\mathrm{H\,I}}$ region.

Table 4 summarizes the results for the fit parameters $\log A$ and β for different column density regions and interval widths.

Of course the choice of the size of the intervals $\Delta \log N_{\mathrm{H\,I}}$ in which the lines are collected is somewhat arbitrary. Figure 4 is based on a larger step size $\Delta \log N_{\mathrm{H\,I}} = 0.5$. For $\log N_{\mathrm{H\,I}} = 13.00-16.50$, the distribution can be well approximated by $\beta = 1.63 \pm 0.02$ (again weighted with $\sigma_{\log f}^2$). This is

Table 5. Fit parameters of the column density distribution for different redshift ranges. Indicated are (*from left to right*): the z interval; the $\log N_{\mathrm{H\,I}}$ range of the data points considered in the fit; the fit parameters $\log A$ and β with their 1σ errors.

z	$\log N_{\mathrm{H\,I}}$	$\log A$	β
0.5–1.0	12.90–15.70	9.1 ± 0.7	1.57 ± 0.05
1.0–1.5	12.90–15.70	9.1 ± 0.5	1.58 ± 0.04
1.5–2.0	12.90–15.70	8.7 ± 0.6	1.55 ± 0.04

within 1σ consistent with the slope for the interval width 0.1 in the comparable range $\log N_{\mathrm{H\,I}} = 12.90-17.20$ (only two lines lie in the interval $\log N_{\mathrm{H\,I}} = 16.50-17.20$), which makes the point that the choice of the interval width does not influence the result.

Frequently a dependence of the index β on z has been postulated by observers (Kim et al. 1997, 2001, 2002; Davé & Tripp 2001; Heap et al. 2002; Misawa 2002). Davé & Tripp (2001) found $\beta = 2.04 \pm 0.23$ and Heap et al. (2002) derived $\beta = 2.02 \pm 0.21$ for $z \sim 0$ each, while Kim et al. (2001) calculated $\beta = 1.72 \pm 0.16$ for $\langle z \rangle = 1.6$ and $\beta = 1.38 \pm 0.08$ for $\langle z \rangle = 2.1$, Telfer et al. (2002) got $\beta = 1.41 \pm 0.05$ for $\langle z \rangle \sim 2.3$ and Hu et al. (1995) and Kim et al. (1997) found $\beta = 1.46$ and $\beta = 1.4$, respectively, both for $\langle z \rangle \sim 3$ (all values calculated for the low column density region $\log N_{\mathrm{H\,I}} \leq 14$ where the number of lines make a reliable judgement possible). Simulations of Theuns et al. (1998), e.g., suggested a clear relationship $\beta(z)$, too. These results are contradicted by the comparatively low gradients of Penton et al. (2000, 2004) for the local universe ($\beta = 1.72 \pm 0.06$ and $\beta = 1.65 \pm 0.07$, respectively). However, the difference might be caused by the analysis method since Penton et al. (2000, 2004) assumed a constant Doppler parameter for the line fits.

In order to search for a possible dependence $\beta(z)$, we examined the column density distribution function separately for three z intervals of the same width (0.5–1.0, 1.0–1.5, 1.5–2.0). For this purpose, the LOS to the quasars had to be divided according to the chosen z intervals, and the absorption distance ΔX had to be computed for the individual intervals following (2). We selected $\Delta \log N_{\mathrm{H\,I}} = 0.1$ for the interval width. The distributions for all three redshift regions and the fits to them are presented in Fig. 5. In each case the fits take into account the points in the interval $\log N_{\mathrm{H\,I}} = 12.90-15.70$. Obviously, the fit parameters given in Table 5 are independent of the redshift range. The increase of β from $z = 1.5-2.0$ ($\beta = 1.55 \pm 0.04$) to $z = 1.0-1.5$ ($\beta = 1.58 \pm 0.04$) represents at best a marginal trend which is not statistically significant.

Fig. 5. Distributions of the Ly α column densities in intervals $\Delta \log N_{\mathrm{H\,I}} = 0.1$, statistical errors of $\log f$ and fits to the distributions for different redshift intervals. Only the data points within the range $\log N_{\mathrm{H\,I}} = 12.90-15.70$ are considered for the fits; they are weighted with the error of $\log f$.

5.2. Distribution of Doppler parameters

To investigate the distribution of the Doppler parameters, we counted the number of lines per Doppler parameter interval in interval widths $\Delta b = 5$ km s^{-1}. Figure 6 shows how b is distributed across the complete line sample (without the 24 broadest lines with $b > 100$ km s^{-1}). The distribution has a typical form: nearly Gaussian with a maximum at $b = (20-25)$ km s^{-1}, an average value $\overline{b} = (34 \pm 22)$ km s^{-1} lying above the maximum, and a long tail to higher Doppler widths. A large fraction of the lines with $b > 100$ km s^{-1} might represent unresolved blends of several components, whereas the steep decline at small Doppler parameters is caused by the SL limit (lines with small b values have small equivalent widths and are more likely to be missed) and by our Ly α selection threshold $b > 10$ km s^{-1}.
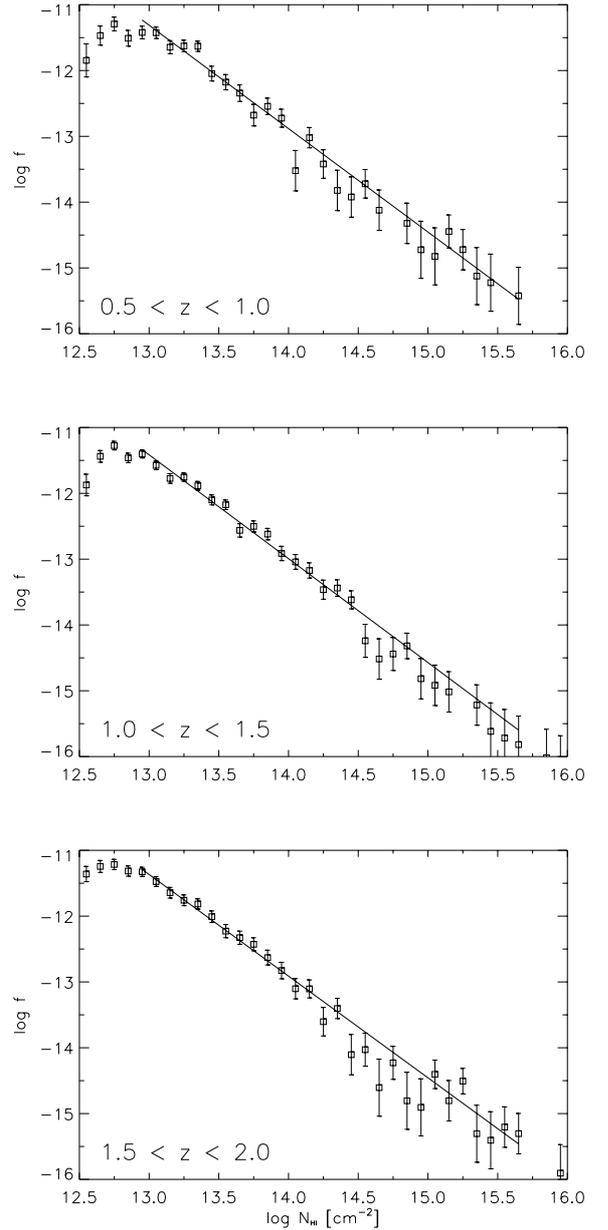
The average and median of b fit the results from other studies in comparable redshift regions very well: Kim et al. (2001) found $b_{\mathrm{median}} = 28$ km s^{-1} for $\langle z \rangle = 1.6$, while Kim et al. (2002) derived $\overline{b} = 32.6$ km s^{-1} for $\langle z \rangle = 2.2$.

Frequently a dependence $b(z)$ is claimed in the sense of a Doppler width increasing with decreasing redshift. In the high redshift range Lu et al. (1996) found $\overline{b} = (23 \pm 8)$ km s^{-1} for $\langle z \rangle = 3.7$, Kim et al. (1997) derived $b_{\mathrm{median}} = 26$ km s^{-1} for $\langle z \rangle = 3.35$ and $b_{\mathrm{median}} = 30$ km s^{-1} for $\langle z \rangle = 2.31$, respectively, and Hu et al. (1995) found $\overline{b} = (28 \pm 10)$ km s^{-1} for $\langle z \rangle = 2.9$. The average value of this study for $\langle z \rangle = 1.31$ appears to support this trend. Going to $z = 0$, the evolution of b possibly continues: Penton et al. (2000) derived $\overline{b} = (38 \pm 16)$ km s^{-1} for the local universe.
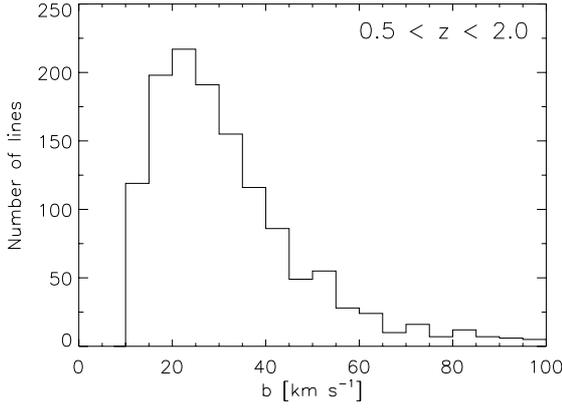
Fig. 6. Distribution of the Ly α Doppler parameters in intervals $\Delta b = 5$ km s^{-1}.

Table 6. Parameters of different b distributions. We give the number of Ly α lines detected, the average value, the median of b, and on the right a parameter that represents the mode.

z	n	$\overline{b}$ [km s^{-1}]	b_{median} [km s^{-1}]	b_σ [km s^{-1}]
0.5−2.0	1325	34 ± 22	28	22.7
0.5−1.0	270	35 ± 23	29	18.9
1.0−1.5	595	33 ± 22	28	23.5
1.5−2.0	460	34 ± 22	28	23.5

Therefore we investigated whether an evolution of b with z can be determined within the z range examined here. In Fig. 7 the b distribution is shown for three different z ranges of the same width, while Table 6 gives parameters of the distributions. The highest average value $\overline{b} = (35 \pm 23)$ km s^{-1} for the interval $z = 0.5{-}1.0$ lies only marginally above those in the higher redshift regions. We see no evolution in the b mean and median over redshifts 0.5 to 2. In general, the question of whether the Doppler width changes with z is not resolved: Kim et al. (2002) also did not see any evolution of $\overline{b}$ in the interval $\langle z \rangle = 3.3 \rightarrow 2.1$ in their data, nor did Davé & Tripp (2001) ($\overline{b} = 25$ km s^{-1} for $\langle z \rangle = 0.2$), whose results do not fit the evolution pattern outlined above.

In addition to the mean and median, we also list a parameter that represents the mode, or most common b value, because this tends to be less sensitive to the S/N and the details of line and continuum fitting. We list values for the parameter $b_\sigma = 1.0574 \cdot b_{\mathrm{peak}}$ from Hui & Rutledge (1999). Tytler et al. (2004) and Jena et al. (2005) found that the Hui & Rutledge (1999) fitting formula with a single parameter $b_\sigma = (23.6 \pm 1.5)$ km s^{-1} gives excellent fits to the b distribution at $1.5 < z < 2.4$. Here we obtain essentially the same value for our two higher redshift bins, 1.0−1.5 and 1.5−2.0, and a smaller value at lower redshifts 0.5−1.0. The b value distribution is significantly wider than the fitting function for the two lower redshift bins, and hence these two b_σ values are not well determined. Both these two lower redshift bins show many more lines with $b < 15$ km s^{-1} than we see at $z > 1.5$. We know, for example from Kirkman et al. (2005), that as the S/N of a spectrum drops, as it does here dramatically at low z, we will measure an excess of both low and high b values. Hence, all the changes that we see may arise from the changing S/N. We do not claim to detect any change in the *intrinsic b* distribution with z.
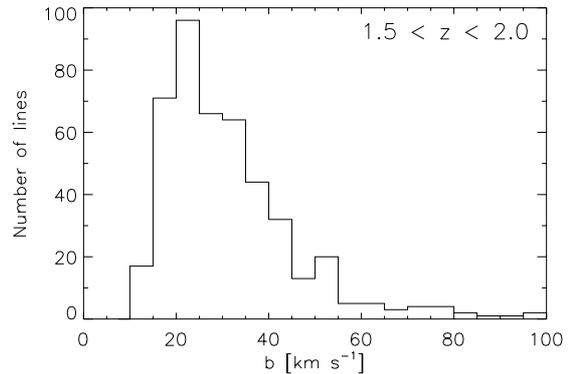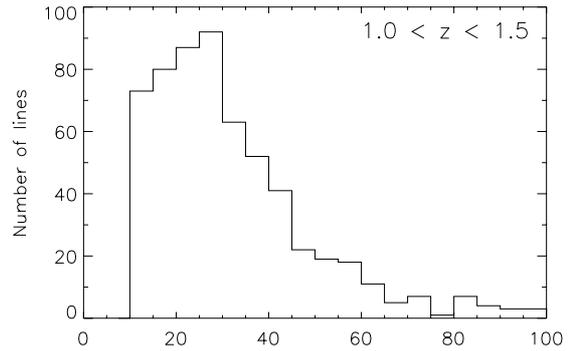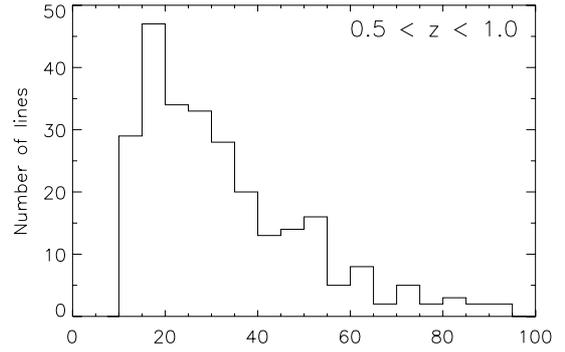

Fig. 7. Distribution of the Ly α Doppler parameters in intervals $\Delta b = 5$ km s^{-1}, varying redshift ranges.

5.3. Clustering of Ly α absorbers

The clustering properties of the baryonic matter can be investigated by computing the correlation between the Ly α absorbers along the LOS. The degree of clustering of the H I absorbers can be expressed by the two-point velocity correlation function

$$\xi(\Delta v) = \frac{n_{\mathrm{obs}}(\Delta v)}{n_{\mathrm{sim}}(\Delta v)} - 1 \qquad (7)$$

(Sargent et al. 1980) where n_{obs}, the number of observed Ly α line pairs in a given velocity separation bin Δv, is compared with the number of expected line pairs n_{sim} derived in the same velocity difference bin in a spectrum with randomly placed lines. For two absorbers at the redshifts z_1 and z_2, the velocity interval at mean redshift in the rest frame is given by

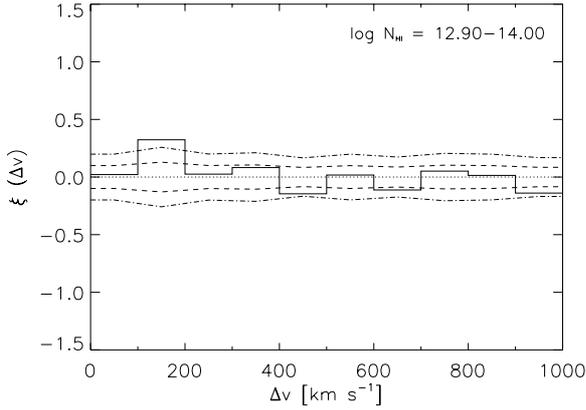$$\Delta v = \frac{c(z_2 - z_1)}{1 + \frac{z_1 + z_2}{2}}. \qquad (8)$$

Fig. 8. Two-point velocity correlation function for the weaker absorbers, up to $1000\ \mathrm{km\,s^{-1}}$, in $100\ \mathrm{km\,s^{-1}}$ bins. The correlation function is shown by the solid line. For orientation $\xi = 0$ is marked with a dotted line. Dashed and dot-dashed lines represent the 1σ and 2σ Poisson errors, related to $\xi = 0$, respectively.

We determined n_{sim} from Monte Carlo simulations by distributing our line sample – in accordance with the derived number density evolution (see Sect. 5.4) – randomly over the spectrum, counting the line pairs for various velocity splittings, repeating this procedure 1000 times, and computing the average.

When the clustering properties in multiple LOS are investigated, each quasar spectrum must first be analyzed separately. Subsequently, the individual numbers of pairs n_{obs} and n_{sim} of the j analyzed LOS can be added in order to build a total ξ based on improved statistics:

$$\xi(\Delta v) = \frac{\sum_{i=1}^{j} n_{\mathrm{obs},i}(\Delta v)}{\sum_{i=1}^{j} n_{\mathrm{sim},i}(\Delta v)} - 1. \qquad (9)$$

For varying intervals Δz and $\Delta \log N_{\mathrm{H\,I}}$, we counted n_{obs} and simulated n_{sim} for every LOS. To investigate the clustering on small scales, we chose $\Delta v_{\mathrm{max}} = 1000\ \mathrm{km\,s^{-1}}$ using a binning of $100\ \mathrm{km\,s^{-1}}$, and we defined $\Delta v_{\mathrm{max}} = 10\,000\ \mathrm{km\,s^{-1}}$ (in $1000\ \mathrm{km\,s^{-1}}$ bins) for a study of the long-scale clustering properties. We calculated ξ according to (9) with $j = 10$ (because the LOS to HS 0747+4259 was formally treated as two LOS: one for $z < 1.44$ and one for $z > 1.56$; compare with Table 3). We estimated the error on the clustering signal with error propagation, assuming a Poisson error for n_{sim} and setting $\sigma_{n_{\mathrm{obs}}} = 0$. We think that this is an acceptable approximation because $\sigma_{n_{\mathrm{obs}}}$ follows directly from σ_λ or σ_z, respectively, and the line positions are very well known compared with the values of the investigated line separations Δz. Furthermore, n_{obs} and n_{sim} have similar values in most cases.

Since Cristiani et al. (1995) found that clustering is stronger for higher column density absorbers, we also looked for this trend. We took the conventional definition $\log N_{\mathrm{H\,I}} > 13.64$ for the strong lines, and we chose $\log N_{\mathrm{H\,I}} = 12.90 - 14.00$ for the low column density absorbers in accordance with the completeness limit of our column density distribution function (see Sect. 5.1).

In Figs. 8 and 9 we show $\xi(\Delta v)$ for the low column density absorbers on scales up to $1000\ \mathrm{km\,s^{-1}}$ and $10\,000\ \mathrm{km\,s^{-1}}$, respectively. We detect a marginal signal above the 2σ level only for $\overline{\Delta v} = 150\ \mathrm{km\,s^{-1}}$, $1500\ \mathrm{km\,s^{-1}}$ and $6500\ \mathrm{km\,s^{-1}}$. Apart from that, $\xi(\Delta v)$ is always below the 1σ level. The excess at $\overline{\Delta v} = 150\ \mathrm{km\,s^{-1}}$ ($\xi = 0.32$, $1\sigma = 0.13$) suggests a clustering of the weak lines over short distances. The signal at $\overline{\Delta v} = 50\ \mathrm{km\,s^{-1}}$
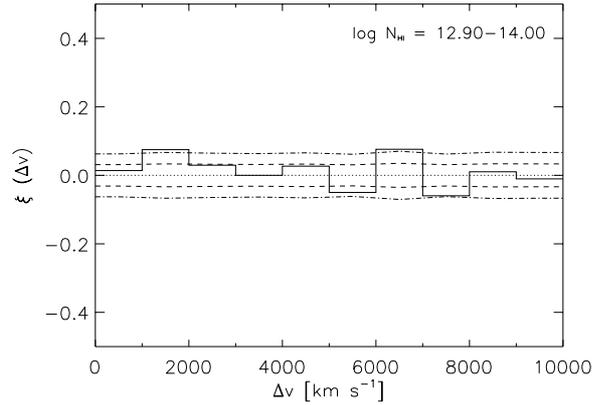

Fig. 9. Two-point velocity correlation function for the weaker absorbers, up to $10\,000\ \mathrm{km\,s^{-1}}$, in $1000\ \mathrm{km\,s^{-1}}$ bins. Line symbols are the same as in Fig. 8.
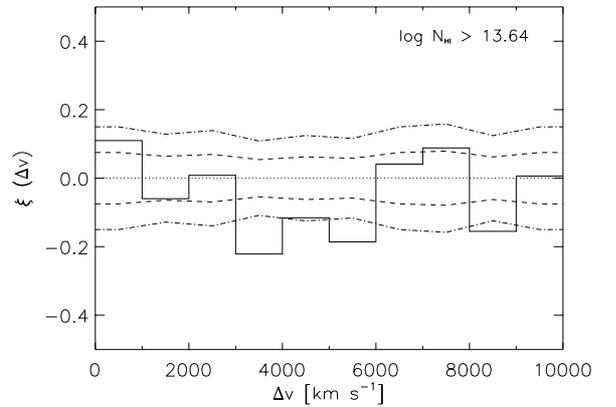
Fig. 10. Two-point velocity correlation function for the stronger absorbers, up to $10\,000\ \mathrm{km\,s^{-1}}$, in $1000\ \mathrm{km\,s^{-1}}$ bins. Line symbols are the same as in Fig. 8.
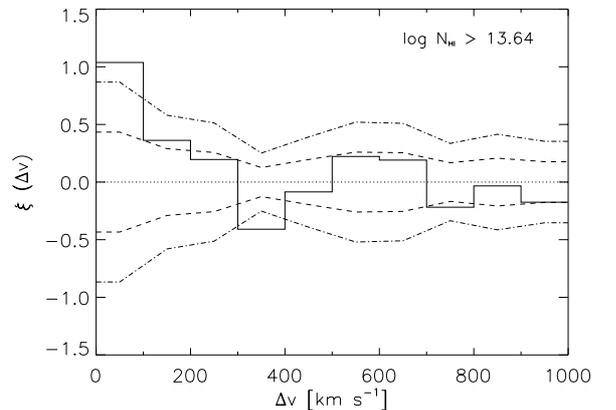
Fig. 11. Two-point velocity correlation function for the stronger absorbers, up to $1000\ \mathrm{km\,s^{-1}}$, in $100\ \mathrm{km\,s^{-1}}$ bins. Line symbols are the same as in Fig. 8.

($\xi = 0.02$, $1\sigma = 0.10$) might be too weak because some weaker lines remain unidentified due to blends: resolving these blends into superpositions of several lines would result in far more line pairs at low Δv.

As expected, we also found slight clustering signals for the high column density absorbers, however only over short distances: $\xi = 1.04 > 2\sigma$ for $\overline{\Delta v} = 50\ \mathrm{km\,s^{-1}}$ and $\xi = 0.36 > 1\sigma$ for $\overline{\Delta v} = 150\ \mathrm{km\,s^{-1}}$ (Fig. 11). At higher distances (up to
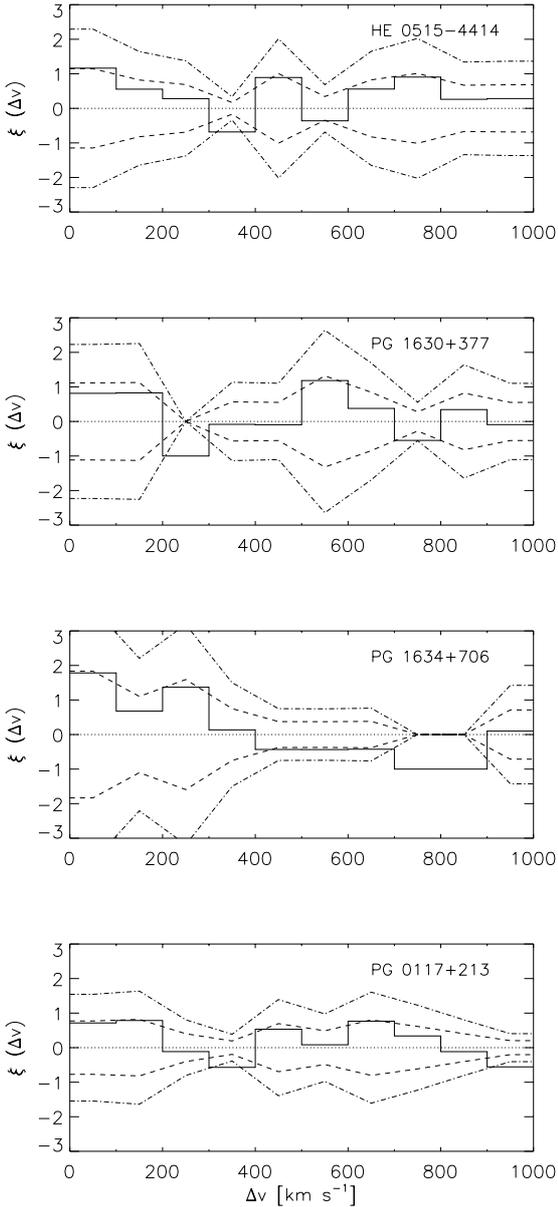
Fig. 12. Two-point velocity correlation function for the stronger absorbers for individual quasar LOS, in 100 km s^{-1} bins. Line symbols are the same as in Fig. 8. When there are no pairs in a specific bin, formally $n_{obs} = 0$, $\xi = -1$, and the 1σ and 2σ Poisson errors are 0, following error propagation as was done for all other bins.

1000 km s^{-1}), the strong absorbers are obviously uncorrelated. The large-scale investigation of the stronger lines provides marginal signals exceeding the 1σ level at $\overline{\Delta v} = 500$ km s^{-1} and $\overline{\Delta v} = 7500$ km s^{-1} (Fig. 10).

The clustering of the high and low column density absorbers on short scales contradicts our own results presented in Janknecht et al. (2002), where no clustering signal at all was found in the LOS to HE 0515-4414 alone, independent of the investigated column density ranges and velocity splittings. Individual LOS might not offer a sufficient statistical basis to detect a weak clustering signal. This is supported by Fig. 12 where we plot the correlation function ξ for some individual LOS of our sample. Although the four LOS with the highest numbers of strong lines are considered (>40), occasionally an

at most marginal excess above the 1σ level can be seen for $\Delta v < 200$ km s^{-1}, but no value at all above the 2σ level.

Most studies found significant clustering on short scales, even to some extent for the low column density lines (Kim et al. 2001; Cristiani et al. 1995; Ulmer 1996; Hu et al. 1995).

Previous observations suggested a clustering signal increasing with decreasing redshift (Kim et al. 2001; Ulmer 1996). This is made plausible by the fact that the structures in the universe develop by gravitational pull over the course of time. In addition, at low redshift $\gtrsim 1/3$ of all Ly α absorbers are associated with galaxies (Lanzetta et al. 1995) which are known to cluster on these scales.

We also searched for a dependence of the correlation function on z. For this purpose, we defined three z intervals of the same width (0.5–1.0, 1.0–1.5 and 1.5–2.0). As described above we computed ξ and estimated the 1σ and 2σ errors separately for each z interval and for distances up to $\Delta v_{max} = 1000$ km s^{-1} in 100 km s^{-1} bins. The results are illustrated in Figs. 13 and 14. For the weaker lines, the $\xi \approx 0$ value for $\Delta v < 100$ km s^{-1} is again probably caused by blending effects, while for $\Delta v > 200$ km s^{-1} no clustering signal can be recognized. For $\overline{\Delta v} = 150$ km s^{-1} the strongest clustering is found in the highest redshift range: $\xi = 0.44 > 2\sigma$. At lower z, ξ is roughly at the 1σ level ($\xi = 0.18$, $1\sigma = 0.19$ for $z = 1.0$–1.5; $\xi = 0.33$, $1\sigma = 0.30$ for $z = 0.5$–1.0), i.e., for $z < 1.5$, ξ doesn't change relative to σ.

The high column density lines show a similar picture for $\overline{\Delta v} = 50$ km s^{-1}: starting at a $\sim 2\sigma$ level ($\xi = 1.40$, $1\sigma = 0.79$), the clustering degree decreases strongly with decreasing redshift. However, the opposite trend can be seen at $\overline{\Delta v} = 150$ km s^{-1} where the signal increases from $\xi \approx 0$ to $\xi \approx 1.5 \sigma$ when going from the highest to the middle z interval. Besides, neither the high nor the low column density absorbers show a clustering signal lying clearly above the 2σ level.

In summary, no uniform evolutionary behaviour of ξ can be established. The rising correlation of the absorbers with decreasing redshift suggested by Kim et al. (2001) and Ulmer (1996) cannot be confirmed.

5.4. Evolution of the number density

As for the clustering properties, a different behaviour is also expected for the number density evolution of the stronger and weaker Ly α lines. We analyze this evolution using the two column density ranges from Sect. 5.3 separately.

In practice, the value for the differential number density $\frac{dn}{dz}$ can be deduced by choosing an interval width Δz and counting the number of absorption lines n in the individual intervals. When the line samples of several LOS which in general cover different z regions are combined, it must be taken into account, of course, that a varying number of LOS n_L falls into a certain redshift interval. (Here, n_L can be estimated from Fig. 1). Thus, we defined a density $\frac{dn}{dz}$ per LOS. Since the fluctuations between the LOS are large, only z intervals with $n_L > 1$ were considered. This is the case for $0.7 \leq z \leq 1.9$.

We computed $\frac{dn}{dz}$ for the two sub-groups as a function of z. On the basis of the Levenberg Marquard algorithm, we fit the power law (1) to the data points of $\frac{dn}{dz}(z)$ and determined $\left(\frac{dn}{dz}\right)_0$ and γ in this way.

Figures 15 and 16 show the data points for the low and high column density absorbers, respectively. In addition to the data points, the best fits to them with their 2σ confidence limits are presented.
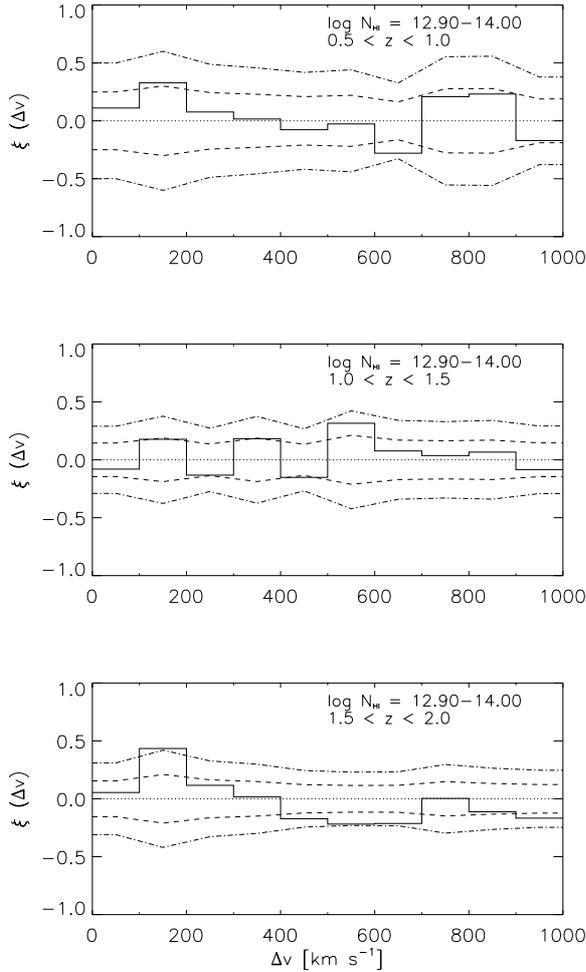
Fig. 13. Evolution of the two-point velocity correlation function for the weaker absorbers, in $100 \ \mathrm{km \, s^{-1}}$ bins, illustrated with three different z intervals. Line symbols are the same as in Fig. 8.

Fig. 14. Evolution of the two-point velocity correlation function for the stronger absorbers, in $100 \ \mathrm{km \, s^{-1}}$ bins, illustrated with three different z intervals. Line symbols are the same as in Fig. 8.

For the weak absorbers, the number density decreases with decreasing redshift with $\gamma = 0.74 \pm 0.31$. The outliers in the interval $z = 0.7 - 0.8$ might be due to the small size of our sample in this region (see Figs. 1 and 2). The stronger lines evolve faster with an exponent $\gamma = 1.50 \pm 0.45$ which is only just consistent (within 1σ) with the exponent of the weak lines.

Figure 17 gives an extensive comparison of the results of this work for the weaker absorbers (here defined by $\log N_{\mathrm{H\,I}} = 13.10 - 14.00$ to facilitate comparison with other results) with different contributions to the number density evolution from the literature measured in varying z regions. Figure 18 does the same for the stronger absorbers. In the double-logarithmic presentations the symbols correspond to the number densities measured in different studies. The Ly α lines of this work are binned in intervals of $\Delta z = 0.2$ in order to have interval sizes comparable with the other investigations. The data points of this study are shown with filled circles; the error bars result from a 1σ poisson error of n.

Regarding the evolution of the weaker absorbers (Fig. 17), it becomes clear that the LOS analyzed here fall into a z region which has not yet been examined so far, due to a lack of high-resolution UV data. The best fit to the data points of this work gives $\gamma = 0.78 \pm 0.27$.

The decrease of the line density with decreasing redshift is obviously decelerated in our investigated z interval, as is
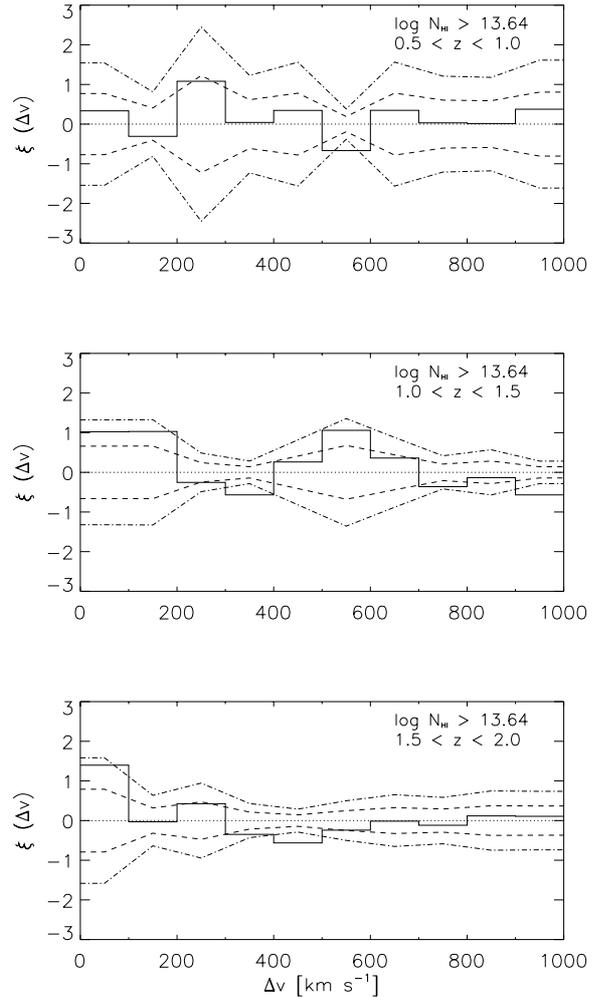
revealed from a comparison with higher redshifts: for $z > 1.5$, Kim et al. (2002) derived $\gamma = 1.18 \pm 0.14$ from a best fit to the data points of different studies (presented as dashed line in Fig. 17). Excluding two LOS, they found $\gamma = 1.42 \pm 0.16$ which is no longer in agreement with the result found here.

Interestingly, an extrapolation of our fit line for $z \to 0$ is consistent within 1σ with the study of Penton et al. (2004) for the local universe (see dotted line in Fig. 17), while an extrapolation of the Kim et al. (2002) fit line misses the Penton et al. (2004) data point by $\approx 2\sigma$. (Williger et al. 2003 examine only a single LOS). We interpret this as further evidence for a changing evolution of the lower column density lines in the interval $z = 1 - 2$.

Furthermore, the comparison with the investigations at higher and at lower z suggests a continuous and moderate transition to the present, rather than a sharp break.

As already derived from Figs. 15 and 16, the high column density absorbers show a steeper gradient in the evolution diagram with $\gamma = 1.66 \pm 0.57$ (Fig. 18). A remarkable data point occupies the interval $z = 0.9 - 1.1$. Without this outlier the evolution index would be much higher and its error much lower ($\gamma = 2.11 \pm 0.21$). A detailed analysis of this redshift range which is covered by six of the nine LOS (see Fig. 1) shows that the high line density is not caused by a fluctuation in an individual LOS, but that the $\frac{dn}{dz}$ lies clearly above the level of the adjacent
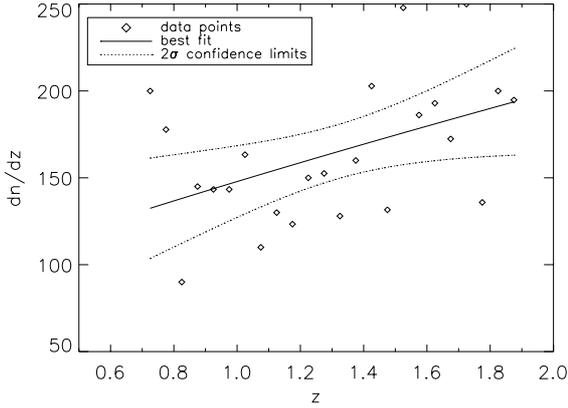
Fig. 15. Number density evolution of the weak Ly α absorbers ($12.90 < \log N_{\mathrm{H\,I}} < 14.00$). Given are the data points (binned with $\Delta z = 0.05$), the best fit and the 2σ confidence limits.
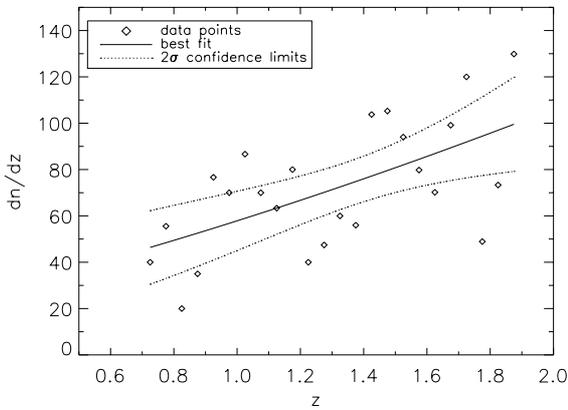

Fig. 16. Same as in Fig. 15, for the strong Ly α absorbers ($\log N_{\mathrm{H\,I}} > 13.64$).

Fig. 17. Comparison of different studies of the number density evolution of the Ly α absorbers with $13.10 < \log N_{\mathrm{H\,I}} < 14.00$. The Ly α lines of this work are binned in $\Delta z = 0.2$ intervals. The solid line represents the best fit to the data points of this work, while the dotted line is an extrapolation of the fit for $z \to 0$. The dashed line shows the best fit to the data points in the higher redshift range, taken from Kim et al. (2002).

Fig. 18. Comparison of different studies of the number density evolution of the Ly α absorbers with $\log N_{\mathrm{H\,I}} > 13.64$. Details as in Fig. 17. The additionally given dashed line for $\log (1 + z) = 0–0.4$ represents the best fit to the data points from Weymann et al. (1998). The data points from Penton et al. (2004), Savaglio et al. (1999) and Williger et al. (2003) apply to $\log N_{\mathrm{H\,I}} > 14.00$.

intervals in nearly all six LOS. Obviously we detect a coincidental line accumulation within this interval.

Just as for the weaker lines, our γ is lower compared with the results of investigations at higher z: Kim et al. (2002) found $\gamma = 2.47 \pm 0.18$ by fitting a straight line to the data points of varying studies for $z > 1.5$ which is inconsistent within 1σ with the value computed here. In addition, the number density continuously decreases in the analyzed range $z = 0.7–1.9$ (apart from the outlier) without showing the frequently postulated break in the evolution at $z = 1.5–1.7$ (Weymann et al. 1998; Dobrzycki et al. 2002; Impey et al. 1996). Possibly this slow-down in the evolution, which was also successfully simulated by theoreticians (Theuns et al. 1998; Davé et al. 1999), takes place in a later phase ($z < 0.7$) beyond the redshift region examined here. An indication for this might be that at lower z the thinning out of the absorbers obviously continues to decelerate: in contrast to the weaker absorbers, an extrapolation of our fit line for $z \to 0$ would lead to a distinctly too low absorber density at $z = 0$, compared with Penton et al. (2004) and Weymann et al. (1998) (see Fig. 18).

If we fit the data points of Weymann et al. (1998) with a straight line (shown in Fig. 18; $\gamma = 0.13 \pm 0.06$), it does not intersect our fit line before $z = 0.6$. Also, leaving out our outlier leads to a point of intersection at $z = 0.8$. Thus, in the case that the break in the number density evolution took place, the redshift value at which it occurred has to be corrected downwards.
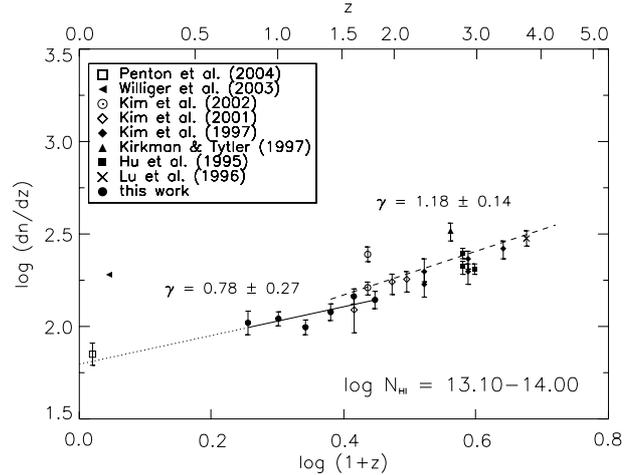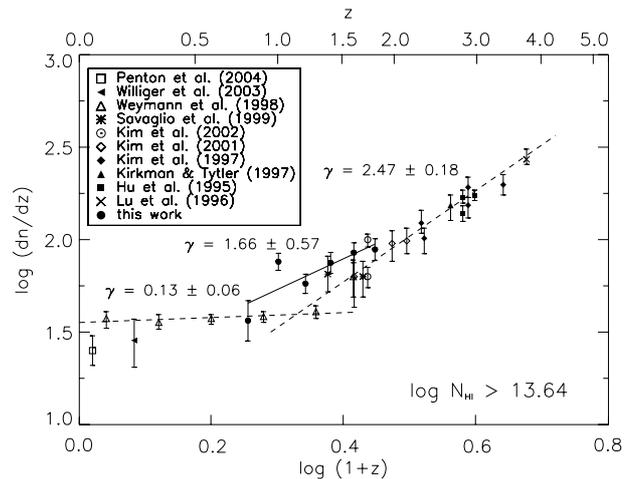
However, it must be noted that Weymann et al. (1998) used the equivalent width W_λ instead of the column density as the observable. The conversion formula

$$W_{\lambda,\mathrm{rest}}\,[\text{Å}] = 8.85 \times 10^{-21} \left(\lambda_{\mathrm{rest}}\,[\text{Å}]\right)^2 f\,N\,\left[\mathrm{cm}^{-2}\right] \qquad (10)$$

(f oscillator strength) only applies to unsaturated absorption lines and depends on the Doppler parameter. Occasionally, $b = 25\,\mathrm{km\,s}^{-1}$ is assumed in the literature (Penton et al. 2000, 2004). Then the lower limit for the equivalent width $W_{\lambda,\mathrm{rest}} = 240\,\mathrm{mÅ}$ used by Weymann et al. (1998) corresponds to a minimum column density $\log N_{\mathrm{H\,I,min}} = 14.00$. Applying this higher cut-off to the evolution diagram of the stronger absorbers would shift our data points in Fig. 18 significantly downwards. As a result of this, the intersection of our fit line with the one to the Weymann et al. (1998) data points (and therefore the evolution break estimated from it) had to be corrected to a higher

redshift. For this reason, the uncertainty in the W_λ–$N_{H\,I}$ conversion makes the exact localization of the slow-down difficult to determine.

Nevertheless, newer studies of Kim et al. (2001), Kim et al. (2002) (whose fit line hits that of the Weymann et al. (1998) data points at $z = 1.1$; see Fig. 18) or Penton et al. (2004) also favoured the break in the evolution taking place at no higher redshift than $z = 1.0$–1.2. Supported by these results, we conclude that a transition in the evolution of the higher column density lines indeed took place, but much later than assumed before. In simulations the sudden slow-down in the evolution results directly from the decline of the UV background at $z = 2$ (Davé et al. 1999). However, the QSO dominated UV background of Haardt & Madau (1996) is usually assumed in these calculations, and thus the contribution of the galaxies is possibly underestimated. With the latter as main source of the UV radiation field for $z < 2$, the radiation field would decrease more slowly and the break would naturally be corrected to a lower z.

All results for the evolution of the number density of Ly α absorbers in this subsection have to be considered in view of the high scatter of the data points. This scatter could not be significantly reduced compared with our study of the single LOS to HE 0515-4414 (Janknecht et al. 2002), though we enhanced the examined total redshift path length Δz by roughly a factor 6. For all nine observed QSOs we obtained high-resolution spectra ($R \geq 30\,000$) where the Ly α forest is completely resolved (because $b_{H\,I} > 10$ km s^{-1}). Therefore, we suppose that the variations from LOS to LOS are caused *physically* (rather than methodically or statistically), reflecting a strongly inhomogenous appearance of the Ly α forest. Indeed, Kim et al. (2002) and Tytler et al. (2004) (for $z < 2.5$ and for $z = 1.9$, respectively) and Impey et al. (1999) for the local universe ($z < 0.2$) found hints for a strong cosmic variance too.

The reason for the large variations of $\frac{dn}{dz}$ between individual LOS falling into the same redshift ranges is probably the advanced stage of structure formation in the universe at $z = 2$. The structures are gravitationally evolved: over- and underdensities have been formed. In individual LOS this can be recognized in the form of strongly varying number densities, in particular of the high column density absorbers. The structure formation obviously starts to dominate over the Hubble expansion, which causes the general decline of the number density.

5.5. Effective optical depth at $z \approx 2$

We examined the effective optical depth τ_{eff} and the average normalized flux $\langle F_{norm} \rangle$, which are related to each other by the equation

$$\tau_{eff} = -\ln \left\langle \frac{F}{F_{cont}} \right\rangle \equiv -\ln \langle F_{norm} \rangle, \tag{11}$$

where F_{cont} is the continuum flux. We calculated τ_{eff} and $\langle F_{norm} \rangle$ for the maximum redshift range of our LOS, $z = 1.81$–1.91. The LOS to three of our quasars fall into the chosen interval: those to HE 2225-2258, HE 0429-4901 and HS 0747+4259 (see Fig. 1). Therefore, we used the flux distributions of the corresponding spectral parts for the calculation of $\langle F_{norm} \rangle$. Because we were interested in the H I absorption of the low density IGM, we defined wavelength regions around the metal lines occuring in the regarded z interval and eliminated these regions from the three spectra. The remaining flux distribution $F(\lambda)$ was divided by the respective continuum flux $F_{cont}(\lambda)$ which is an output parameter

of CANDALF. For the resulting normalized flux averaged over the wavelength positions of all three spectral parts we derived

$$\langle F_{norm} \rangle = 0.895 \pm 0.020 \tag{12}$$

for $\langle z \rangle \approx 1.86$, i.e. 10.5% of the radiative flux is absorbed by the diffuse intergalactic medium at this redshift. The error of $\langle F_{norm} \rangle$ follows from Tytler et al. (2004), Eq. (30): since we have only three LOS, the total error of our average normalized flux is completely dominated by the large scale structure and will probably be >0.02. With (11) and (12) we compute

$$\tau_{eff} = 0.111 \pm 0.020 \tag{13}$$

for the effective optical depth.

Kirkman et al. (2005) investigated the H I opacity of the IGM at $1.6 < z < 3.2$. At $z = 1.86$, the scaling in their Fig. 5 gave $\langle F_{norm} \rangle = 0.889$ with an error of roughly 0.01. Thus, our result agrees with theirs.

6. Conclusions

We have analyzed the combined sample of all Ly α absorption lines which were detected in the spectra of nine quasars over a total redshift path length $\Delta z = 5.176$ within the range $z = 0.5$–1.9. We classified 1325 absorption features as Ly α lines. Examining the distributions of their fit parameters $\log N_{H\,I}$, b and z, we find the following:

1. The column density distribution might be complete down to $\log N_{H\,I} = 12.90$. It can be approximated over roughly three orders of magnitude ($\log N_{H\,I} = 12.90$–15.70) by a simple power law. The slope $\beta = 1.60 \pm 0.03$ is consistent with other studies in comparable redshift intervals. We do not see any change in β with z.
2. The distribution of the Doppler widths has the expected form of nearly Gaussian with an additional expanded tail to high b and an average value $\overline{b} = (34 \pm 22)$ km s^{-1}. We cannot detect any evolution of the Doppler parameter distribution with z in the examined redshift phase.
3. The weaker ($\log N_{H\,I} = 12.90$–14.00) as well as the stronger Ly α lines ($\log N_{H\,I} > 13.64$) show marginal clustering with a 2σ significance on short velocity intervals ($\Delta v < 200$ km s^{-1} and $\Delta v < 100$ km s^{-1}, respectively). However, the clustering signal is too weak to be seen in individual LOS. We do not see any change with column density or redshift.
4. Using the customary power law $\frac{dn}{dz} \propto (1 + z)^\gamma$, the evolution of the number density of the weaker Ly α lines declines with $\gamma = 0.74 \pm 0.31$ with decreasing z within the range $z = 0.7$–1.9. From comparisons with investigations of other authors at higher and lower redshifts we conclude that the decrease of the weaker lines is decelerated in the phase $z = 1$–2, turning into a nearly flat evolution for $z \to 0$, without showing any hint for a sharp break in the evolution.
5. The number density of the stronger absorbers also decreases with decreasing z ($\gamma = 1.50 \pm 0.45$ for $z = 0.7$–1.9), faster than for the weaker lines, though the trends are consistent with each other within 1σ.
6. The decline of the line density of the stronger absorbers is also decelerated compared with higher redshifts ($z = 1.5$–4.0). The break in the evolution predicted for $z = 1.5$–1.7 cannot be detected, however. The deduced z dependence of the number density as well as comparisons with other studies for the local universe rather suggest a later

slow-down ($z < 0.7$), followed by an approximately flat evolution. The precise z value of the break in the evolution probably has to be corrected somewhat upwards due to the uncertain conversion between equivalent width (used by Weymann et al. 1998, as observable) and column density.

7. Though having analyzed nine high-resolution ($R \geq 30\,000$) quasar spectra altogether, the scatter of the data points in the diagrams of the number density evolution is large. As Tytler et al. (2004) showed, the strong variations between the LOS are consistent with the effects of normal structure formation.

8. An analysis of the flux distribution of the three quasars with LOS in the upper redshift range ($z = 1.81-1.91$) gives $\langle F_{\mathrm{norm}} \rangle = 0.895 \pm 0.020$ for the average normalized flux and $\tau_{\mathrm{eff}} = 0.111 \pm 0.020$ for the effective optical depth, in good agreement with the values from Kirkman et al. (2004).

References

Bahcall, J. N., Jannuzi, B. T., Schneider, D. P., et al. 1991, ApJ, 377, L5
Carswell, R. F., Webb, J. K., Baldwin, J. A., & Atwood, B. 1987, ApJ, 319, 709
Caulet, A. 1989, ApJ, 340, 90
Cristiani, S., D'Odorico, S., Fontana, A., Giallongo, E., & Savaglio, S. 1995, MNRAS, 273, 1016
Davé, R., & Tripp, T. M. 2001, ApJ, 553, 528
Davé, R., Hernquist, L., Katz, N., & Weinberg, D. H. 1999, ApJ, 511, 521
Dobrzycki, A., Bechtold, J., Scott, J., & Morita, M. 2002, ApJ, 571, 654
Fontana, A., & Ballester, P. 1995, ESO Messenger, 80, 37
Giallongo, E., Cristiani, S., Fontana, A., & Trèvese, D. 1993, ApJ, 416, 137
Haardt, F., & Madau, P. 1996, ApJ, 461, 20
Heap, S. R., Williger, G. M., Davé, R., et al. 2002, in Extragalactic Gas at Low Redshift, ed. J. S. Mulchaey, & J. Stocke, ASP Conf. Proc., 254, 63
Hu, E. M., Kim, T.-S., Cowie, L. L., Songaila, A., & Rauch, M. 1995, AJ, 110, 1526
Hui, L., & Rutledge, R. E. 1999, ApJ, 517, 541
Impey, C. D., Petry, C. E., Malkan, M. A., & Webb, W. 1996, ApJ, 463, 473
Impey, C. D., Petry, C. E., & Flint, K. P. 1999, ApJ, 524, 536
Janknecht, E., Baade, R., & Reimers, D. 2002, A&A, 391, L11
Jena, T., Norman, M. L., Tytler, D., et al. 2005, MNRAS, 361, 70
Kim, T.-S., Hu, E. M., Cowie, L. L., & Songaila, A. 1997, AJ, 114, 1
Kim, T.-S., Cristiani, S., & D'Odorico, S. 2001, A&A, 373, 757
Kim, T.-S., Carswell, R. F., Cristiani, S., D'Odorico, S., & Giallongo, E. 2002, MNRAS, 335, 555
Kirkman, D., & Tytler, D. 1997, ApJ, 484, 672
Kirkman, D., Tytler, D., Suzuki, N., et al. 2005, MNRAS, 360, 1373
Lanzetta, K. M., Bowen, D. V., Tytler, D., & Webb, J. K. 1995, ApJ, 442, 538
Levshakov, S. A., Agafonova, I. I., Reimers, D., & Baade, R. 2003, A&A, 404, 449
Levshakov, S. A., Agafonova, I. I., Reimers, D., et al. 2005, in From Lithium to Uranium: Elemental Tracers of Early Cosmic Evolution, ed. V. Cill, P. François, & F. Primas (Cambridge University Press), IAU Symp. Proc., 228 597
Lu, L., Sargent, W. L. W., Womble, D. S., & Takada-Hidai, M. 1996, ApJ, 472, 509
Meiksin, A., & Madau, P. 1993, ApJ, 412, 34
Misawa, T., Tytler, D., Iye, M., et al. 2002, AJ, 123, 1847
Misawa, T. 2002, Spectroscopic Analysis of H I Absorption Line Systems in 40 HIRES QSOs, Ph.D. Thesis, Tokio
Noguchi, T., Maehara, H., & Kondo, M. 1980, Tokyo Astronomical Observatory, Annals, Second Series, 18, 55
Penton, S. V., Shull, J. M., & Stocke, J. T. 2000, ApJ, 544, 150
Penton, S. V., Stocke, J. T., & Shull, J. M. 2004, ApJS, 152, 29
Petitjean, P., Webb, J. K., Rauch, M., et al. 1993, MNRAS, 262, 499
Quast, R., Baade, R., & Reimers, D. 2002, A&A, 386, 796
Quast, R., Reimers, D., & Levshakov, S. A. 2004, A&A, 415, L7
Quast, R., Reimers, D., & Baade, R. 2006, A&A, submitted
Reimers, D., Hagen, H.-J., Rodriguez-Pascual, P., & Wisotzki, L. 1998, A&A, 334, 96
Reimers, D., Baade, R., Hagen, H.-J., & Lopez, S. 2001, A&A, 374, 871
Reimers, D., Baade, R., Quast, R., & Levshakov, S. 2003, A&A, 410, 785
Reimers, D., Janknecht, E., Fechner, C., et al. 2005, A&A, 435, 17
Reimers, D., Agafonova, I. I., Levshakov, S. A., et al. 2006, A&A, 449, 9
Sargent, W. L. W., Young, P. J., Boksenberg, A., & Tytler, D. 1980, ApJS, 42, 41
Savaglio, S., Ferguson, H. C., Brown, T. M., et al. 1999, ApJ, 515, L5
Schmidt, M., & Green, R. F. 1983, ApJ, 269, 352
Sembach, K., & Savage, B. D. 1992, ApJS, 83, 147
Shimmins, A. J., Day, G. A., Ekers, R. D., & Cole, D. J. 1966, Austr. J. Phys., 19, 837
Telfer, R. C., Zheng, W., Kriss, G. A., & Davidsen, A. F. 2002, ApJ, 565, 773
Theuns, T., Leonard, A., & Efstathiou, G. 1998, MNRAS, 297, 49
Tytler, D. 1982, Nature, 298, 427
Tytler, D. 1987, ApJ, 321, 49
Tytler, D., & Fan, X. M. 1992, ApJS, 79, 1
Tytler, D., Boksenberg, A., Sargent, W., Young, P., & Kunth, D. 1987, ApJS, 64, 667
Tytler, D., Kirkman, D., O'Meara, J. M., et al. 2004, ApJ, 617, 1
Ulmer, A. 1996, ApJ, 473, 110
de la Varga, A., Reimers, D., Tytler, D., Barlow, T., & Burles, S. 2000, A&A, 363, 69
Weymann, R. J., Jannuzi, B. T., Lu, L., et al. 1998, ApJ, 506, 1
Williger, G. M., Heap, S. R., Weymann, R. J., Davé, R., & Tripp, T. M. 2003, in The IGM/Galaxy Connection, proceedings, ed. J. L. Rosenberg, & M. E. Putman (Kluwer Academic Publishers), 265
Wisotzki, L., Christlieb, N., Bade, N., et al. 2000, A&A, 358, 77
Young, P., Sargent, W. L. W., Boksenberg, A., Carswell, R., & Whelan, J. 1979, ApJ, 229, 891